Orbits of 152 Globular Clusters of the Milky Way Galaxy Constructed from the Gaia DR2 data

A. T. Bajkova, V. V. Bobylev

Pulkovo Astronomical Observatory, St.-Petersburg, Russia, E-mail: bajkova@gaoran.ru

Abstract

We present orbits and their properties for 152 globular clusters of the Milky Way galaxy obtained using average Gaia DR2 proper motions and other astrometric data from the list of Vasiliev (2019). For orbit integrating we have used the axisymmetric model of the Galactic potential based on the Navarro-Frenk-White dark halo, and modified by Bajkova, Bobylev (2016, 2017) using circular velocities of Galactic objects in wide region of Galactocentric distances (up to 200 kpc) from Bhattacharjee et al. (2014) catalog. Based on the analysis of the obtained orbits, we have modified the composition of the subsystems of globular clusters presented in Massari et al. (2019).

Key words: (Galaxy:) globular clusters: general

1   Introduction

The appearance of accurate astrometric data from measurements from the Gaia satellite of the positions and spatial velocities of globular clusters (Helmi et al. 2018; Baumgardt et al. 2019; Vasiliev 2019) makes it possible to study their dynamics, origin and evolution (Myeong et al. 2019; Massari et al. 2019; Bajkova et al. 2020).

In this work we present orbits and their properties for the almost entire list of globular clusters compiled by Vasiliev (2019) on the basis of the most accurate measurements of their velocities and positions to date and using one of the best-fit models of the Milky Way gravitational potential. In addition, we set a goal to revise the classification of globular clusters proposed by Massari et al. (2019) on the basis of analysis of the obtained orbits. In essence, this paper is a supplement to paper of Bajkova et al. (2020), which was devoted to the division of globular clusters into subsystems of the Galaxy, namely, bulge/bar, thick disk, and halo. Recall that in paper of Bajkova et al. (2020) a new criterion of separation of globular clusters belonging to the disk and halo of the Galaxy was proposed. This criterion is based on the bimodality of the GCs distribution L_Z/ecc, where L_Z is Z component of the angular momentum, ecc is eccentricity of the orbit.

In addition to work of Bajkova et al. (2020), we present here a broader set of orbital parameters, and most importantly, we present a catalog of orbit images in two projections, which makes it possible to more fully analyze them due to visualization. Such work on visualization of the orbits of almost all globular clusters known to date, and carried out according to the latest data, has been done in the literature for the first time. This work provides, in addition to the available quantitative estimates, the possibility of a qualitative assessment of the GC dynamics, comparison of the orbits of different GCs included in different classification groups.

In the previous work, we dealt only with the problem of dividing the GCs into formed in situ and clusters which formed in different progenitors that were only later accreted, i.e. division into disk, bulge and halo subsystems. We did not touch upon the problem of classifying the halo GCs into subsystems, the nature of which is the accretion events of members of other galaxies (the Sausage, Sequoia) onto the Milky Way. An attempt at such a classification was made, for example, in the work

of Massari et al. (2019). But we do not consider this work completed, since the analysis of the various diagrams suggests some inconsistencies and contradictions. A qualitative analysis of the orbits allowed us to make some adjustments to the Massari's classification. As a result, we offer our own modified classification, which seems to be more organic. The change in classification affected 27 objects.

In addition to the previous article, we present the values of important orbital parameters that were not considered earlier.

This work is structured as follows. Section 2 describes the accepted most realistic model for the axially symmetric Galactic potential. Section 3 devoted to integrating the orbits and computing parameters of the orbits. Section 4 describes data. In Section 5 we present orbits of 152 globular clusters and their properties and propose a modified classification of the GCs based on the analysis of orbits which is slightly different from the classification given by Massari et al. (2019). In Conclusions we summarize main results.

2 Model for the Axially Symmetric Galactic Potential

In this article the same model of gravitational potential as in work by Bajkova et al. (2020) is adopted. The axially symmetric gravitational potential of the Galaxy is represented as the sum of three components — the central, spherical bulge $\Phi_b(r(R, Z))$, the disk $\Phi_d(r(R, Z))$, and the massive, spherical dark-matter halo $\Phi_h(r(R, Z))$:

$$\Phi(R, Z) = \Phi_b(r(R, Z)) + \Phi_d(r(R, Z)) + \Phi_h(r(R, Z)). \tag{1}$$

Here, we use a cylindrical coordinate system (R, ψ, Z) with its origin at the Galactic center. In Cartesian coordinates (X, Y, Z) with their origin at the Galactic center, the distance to a star (the spherical radius) is $r^2 = X^2 + Y^2 + Z^2 = R^2 + Z^2$. The gravitational potential is expressed in units of 100 km^2 s^{-2}, distances in kpc, masses in units of the mass of the Galaxy, $M_{gal} = 2.325 \times 10^7 M_\odot$, and the gravitational constant is taken to be $G = 1$.

We express the potentials of the bulge, $\Phi_b(r(R, Z))$, and disk, $\Phi_d(r(R, Z))$, in the form suggested by Miyamoto, Nagai (1975):

$$\Phi_b(r) = -\frac{M_b}{(r^2 + b_b^2)^{1/2}}, \tag{2}$$

$$\Phi_d(R, Z) = -\frac{M_d}{\left[R^2 + \left(a_d + \sqrt{Z^2 + b_d^2}\right)^2\right]^{1/2}}, \tag{3}$$

where M_b, M_d are the masses of these components, and b_b, a_d, b_d are the scale parameters of the components in kpc.

For description of the halo component, we used the expression in Navarro-Frenk-White (NFW) form presented in Navarro et al. (1997):

$$\Phi_h(r) = -\frac{M_h}{r} \ln\left(1 + \frac{r}{a_h}\right), \tag{4}$$

where M_h is the mass, a_h is the scale length.

The model of the Galactic potential, considered in this work, is the NFW model modified in work of Bajkova & Bobylev (2016) by fitting of the model parameters to data on HI, maser sources and Galactic objects from Bhattacharjee et al. (2014) at distances R within ~ 200 kpc. In addition the constraints (Irrgang et al. 2013) on the local dynamical matter density $\rho_\odot = 0.1 M_\odot$ pc^{-3} and the force acting perpendicularly to the Galactic plane $|K_{z=1.1}|/2\pi G = 77 M_\odot$ pc^{-2} were used.

Note that among six models of the Galactic potential summarized in Bajkova & Bobylev (2017) our model (denoted as Model III in papers of Bajkova & Bobylev (2016, 2017) ensures the best fit to the data. Here we denote the model as NFWBB for short.

Parameters of the NFWBB model are given in Table 1 of work of Bajkova et al. (2020). Corresponding rotation curves up to $R = 200$ kpc are shown in Fig.3 of work by Bajkova & Bobylev (2016). When deriving the model rotation curve, we used $R_\odot = 8.3$ kpc for the Galactocentric distance of the Sun and $V_\odot = 244$ km s^{-1} for the linear velocity of the Local Standard of Rest around the center of the Galaxy. The mass of the Galaxy according to this model is $M_{G(R \leq 200kpc)} = 0.75 \pm 0.19 \times 10^{12} M_\odot$. This value is consistent with the recently obtained estimate of the lower mass limit for the dark spherical NFW halo $M_{200} = 0.67^{+0.30}_{-0.15} \times 10^{12} M_\odot$ (Koppelman & Helmi, 2020) from the escape velocity using a proper motion selected halo sample.

3   Integrating the Orbits and Computing Orbit Parameters

The equation of motion of a test particle in an axially symmetric gravitational potential can be obtained from the Lagrangian of the system £ (see Appendix A in Irrgang et al. (2013)):

$$£(R, Z, \dot{R}, \dot{\psi}, \dot{Z}) = 0.5(\dot{R}^2 + (R\dot{\psi})^2 + \dot{Z}^2) - \Phi(R, Z). \tag{5}$$

Introducing the canonical moments

$$\begin{aligned} p_R &= \partial £/\partial \dot{R} = \dot{R}, \\ p_\psi &= \partial £/\partial \dot{\phi} = R^2 \dot{\psi}, \\ p_Z &= \partial £/\partial \dot{Z} = \dot{Z}, \end{aligned} \tag{6}$$

we obtain the Lagrangian equations in the form of a system of six first-order differential equations:

$$\begin{aligned} \dot{R} &= p_R, \\ \dot{\psi} &= p_\psi/R^2, \\ \dot{Z} &= p_Z, \\ \dot{p_R} &= -\partial\Phi(R, Z)/\partial R + p_\psi^2/R^3, \\ \dot{p_\psi} &= 0, \\ \dot{p_Z} &= -\partial\Phi(R, Z)/\partial Z. \end{aligned} \tag{7}$$

We integrated Eqs. (7) using a fourth-order Runge-Kutta algorithm.

The Sun's peculiar velocity with respect to the Local Standard of Rest was taken to be $(u_\odot, v_\odot, w_\odot) = (11.1, 12.2, 7.3) \pm (0.7, 0.5, 0.4)$ km s^{-1} ((Schonrich et al. 2010)). Here, we use the heliocentric velocities in a moving Cartesian coordinate system with u directed towards the Galactic center, v in the direction of the Galactic rotation, and w perpendicular to the Galactic plane and directed towards the north Galactic pole.

Let the initial positions and space velocities of a test particle in the heliocentric coordinate system be $(x_o, y_o, z_o, u_o, v_o, w_o)$. The initial positions (X, Y, Z) and velocities (U, V, W) of the test particle in Galactic Cartesian coordinates are then given by the formulas:

$$\begin{aligned} X &= R_\odot - x_o, Y = y_o, Z = z_o + h_\odot, \\ R &= \sqrt{X^2 + Y^2}, \\ U &= u_o + u_\odot, \\ V &= v_o + v_\odot + V_\odot, \\ W &= w_o + w_\odot, \end{aligned} \tag{8}$$

where $R_\odot$ and $V_\odot$ are the Galactocentric distance and the linear velocity of the Local Standard of Rest around the Galactic center, $h_\odot = 16$ pc (Bajkova & Bobylev, 2016) is the height of the Sun above the Galactic plane, Π and Θ are radial and tangential (rotational) velocities respectively.

Below we present the following orbital parameters of globular clusters:

(1)initial distance of the GC from the Galactic center d_{GC}:

$$d_{GC} = \sqrt{X^2 + Y^2 + Z^2}; \tag{9}$$

(2)radial velocity Π:

$$\Pi = -U\frac{X}{R} + V\frac{Y}{R}; \tag{10}$$

(3)tangential velocity Θ:

$$\Theta = U\frac{Y}{R} + V\frac{X}{R}; \tag{11}$$

(4)total 3D velocity V_{tot}:

$$V_{tot} = \sqrt{\Pi^2 + \Theta^2 + W^2}; \tag{12}$$

(5)apocentric distance (apo) of the orbit;
(6)pericentric distance (peri) of the orbit;
(7)the eccentricity (ecc) of the orbit:

$$ecc = \frac{apo - peri}{apo + peri}; \tag{13}$$

(8)the components of the angular momentum:

$$L_X = Y \times W - Z \times V; \tag{14}$$

$$L_Y = Z \times U - X \times W; \tag{15}$$

$$L_Z = X \times V - Y \times U; \tag{16}$$

(9)inclination of the orbit θ:

$$\theta = \arccos(\frac{L_Z}{L}), \tag{17}$$

where $L = \sqrt{L_X^2 + L_Y^2 + L_Z^2}$;
(10)period of the orbit T_r;
(11)total energy E:

$$E = \Phi(R, Z) + \frac{V_{tot}^2}{2}. \tag{18}$$

4   Data

In this paper, as the source of data on globular clusters the Vasiliev (2019) catalog serves. It contains average proper motions calculated from data of the Gaia DR2 Catalog, line-of-sight velocities, (α, δ) positions and distances of 150 globular clusters. Data for GC Liller 1 we took from previous preprint of Vasiliev (2018). For the globular cluster FSR 1758, we took data from the work of Villanova et al. (2019).

The initial position and velocity coordinates (the 6d phase space) $(x_o, y_o, z_o, u_o, v_o, w_o)$ were calculated from these data and used for integrating the orbits. Uncertainties in the initial coordinates were

calculated using Monte-Carlo simulation (1000 iterations) taking into account the measurement errors given in catalog of Vasiliev (2019). We adopted the uncertainty in the GCs heliocentric distances d as 7%, which is about 1.5 times larger than the estimate given by Vasiliev (2019).

Actually, Vasiliev (2019) used the distances from the Harris (2010) catalog, where it is assumed an error of 0.1 in distance modulus, corresponding to a relative error of 4.6% in the distance, which, according to Vasiliev (2019), is a rather optimistic choice, since for some clusters, as follows from independent literature sources, the variation in several independent distance estimates could exceed 0.1 mag. It should be borne in mind that there is a possibility of additional error due to inhomogeneity in absorption in the Galaxy, but this is unlikely to give a contribution greater than 0.1 mag (color excess error $E(B - V) \sim 0.03$). Hence, the total error (square root of the sum of squares) in the distance modulus is hardly more than 0.15 mag, which corresponds to about 7% uncertainty in the distances.

Even in the case of an estimate of 4.6%, the distance seems to be the largest source of uncertainty for most of the clusters (Vasiliev (2019)), the more this is aggravated in our case, when the uncertainty in the distances is assumed to be about 1.5 times larger (7%). Therefore, it makes sense to study the effect of distance uncertainties on the values of the clusters orbit parameters. Comparison of the most important orbit parameters $(E, L_Z, ecc, L_Z/ecc, V_{tot}, Apo, \theta, T_r)$ is given in Fig. 1. In this Figure the parameters obtained for the GCs with the distances which are both larger on 7% and less on 7% than the nominal ones, are compared with the corresponding orbit parameters obtained for the GCs with nominal distances.

It should be especially noted that among the analyzed parameters we also included the ratio L_Z/ecc, the bimodality of the distribution of which we used in work of Bajkova et al. (2020) to separate globular clusters belonging to the thick disk and halo. The influence of the uncertainty in the GC distances of 7% led to a standard deviation of this ratio of 5% (relative to effective range of this parameter), which we expect did not affect the result of GCs classification due to the high stability of the separation algorithm shown in work of Bajkova et al. (2020). The greatest influence from uncertainty in distances of 7% is experienced by such parameters as eccentricity (ecc) and inclination of orbit θ. The standard deviations of these parameters are 7.6 and 8.4%, respectively. All other parameters are significantly less influenced, with a standard deviation of not larger than 3% in each case.

5   Orbits of 152 Globular Clusters and their Properties

The orbits of the 152 globular clusters were obtained by integrating Eg. (7) for 5 Gyr backward. The (X,Y) and (R,Z) orbit projections for each of all GCs are presented in Fig. 2. The orbit properties are presented in Table 1. To calculate the uncertainties in the orbit properties, we used the Monte Carlo method with 100 realizations, taking into account the uncertainties in the initial coordinates and velocities of GCs, as well as errors in the peculiar velocity of the Sun. For parameters T_r, L_Z and E, we give in Table 1 only nominal values to save space.

Based on the analysis of orbits and their properties, a small regrouping of globular clusters by subsystems has been made. Table 2 shows 27 GCs, which have changed their belonging to one group or another. In this table, the column designated as GS – Galactic Subsystem, gives the classification proposed by Massari et al. (2019), and the column designated as GS(m), gives a modified classification. The following designations for the Galactic subsystems are used here: D (disk), B (bulge), GE (Gaia-Enceladus, or Gaia-Sausage), H99 (Helmi Streams), Seq (Sequoia galaxy), Sgr (Sagittarius dwarf), HE (unassociated High-Energy), LE (unassociated Low-Energy), XXX (clusters with no available kinematics).
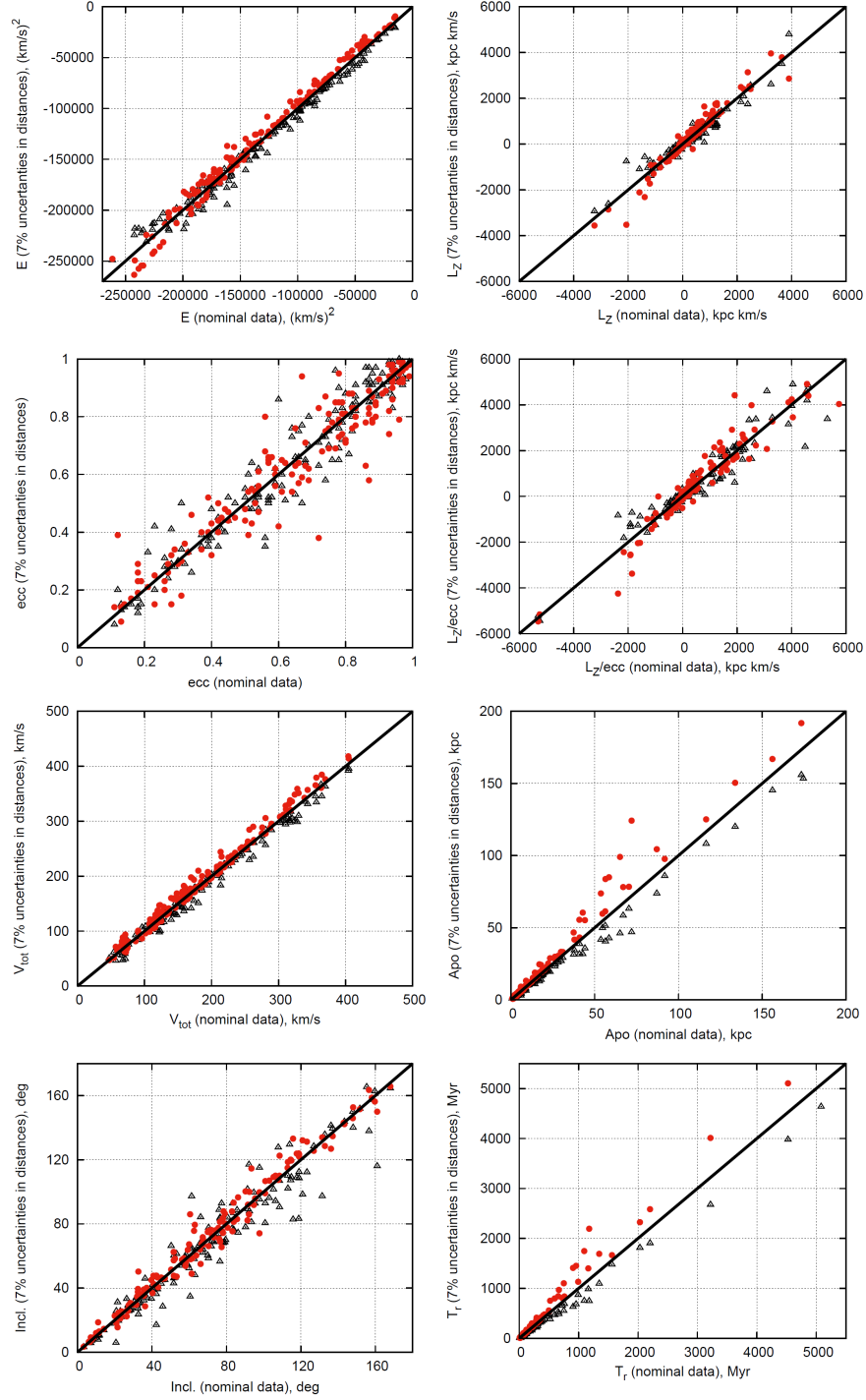
Figure 1: Comparison of the GCs orbit parameters $(E, L_Z, ecc, L_Z/ecc, V_{tot}, Apo, \theta, T_r)$. The parameters obtained for the GCs with the distances which are larger on 7% (red points) and less on 7% (black triangles) than the nominal ones, are compared with the corresponding orbit parameters obtained for the GCs with nominal distances. In each panel we plot the line of coincidence.

Table 1: Orbital properties of the GCs. For each GC we quote values derived from orbits integrated for 5 Gyr backward.

Name	d_{GC} [kpc]	Π [km/s]	Θ [km/s]	V_{tot} [km/s]	apo [kpc]	peri [kpc]	ecc	incl. θ [deg]	T_r [Myr]	L_Z [kpc km/s]	E [km²/s²]
NGC 104	7.6	6^{+5}_{-9}	192^{+8}_{-3}	197^{+7}_{-3}	$7.7^{+0.1}_{-0.1}$	$5.5^{+0.3}_{-0.2}$	$0.16^{+0.02}_{-0.03}$	27^{+2}_{-1}	116	1328	-126288
NGC 288	12.2	9^{+3}_{-4}	-42^{+28}_{-22}	66^{+16}_{-14}	$12.3^{+0.3}_{-0.4}$	$1.4^{+0.7}_{-0.8}$	$0.80^{+0.11}_{-0.10}$	119^{+7}_{-16}	142	-349	-116280
NGC 362	9.5	127^{+18}_{-13}	-1^{+12}_{-12}	145^{+16}_{-9}	$12.1^{+0.3}_{-0.6}$	$0.1^{+0.3}_{-0.0}$	$0.99^{+0.00}_{-0.06}$	92^{+22}_{-19}	126	-10	-121290
Whiting 1	34.7	-208^{+18}_{-14}	109^{+22}_{-16}	235^{+18}_{-17}	$67.0^{+14.3}_{-9.0}$	$20.3^{+3.4}_{-1.3}$	$0.54^{+0.02}_{-0.05}$	67^{+3}_{-2}	1162	2494	-42265
NGC 1261	18.2	-95^{+11}_{-9}	-19^{+10}_{-9}	119^{+9}_{-8}	$21.1^{+1.4}_{-1.0}$	$0.7^{+0.4}_{-0.2}$	$0.94^{+0.03}_{-0.04}$	121^{+11}_{-16}	244	-249	-91385
Pal 1	17.4	42^{+6}_{-8}	214^{+3}_{-4}	219^{+3}_{-3}	$19.1^{+0.4}_{-0.9}$	$14.6^{+0.6}_{-0.8}$	$0.13^{+0.03}_{-0.02}$	14^{+1}_{-1}	350	3646	-78086
E 1	124.7	11^{+75}_{-72}	-144^{+114}_{-88}	174^{+104}_{-45}	$237.9^{+45.2}_{-42.9}$	$104.3^{+30.3}_{-45.9}$	$0.39^{+0.41}_{-0.00}$	127^{+6}_{-28}	5594	-12100	-15914
Eridanus	95.2	-90^{+27}_{-31}	-28^{+48}_{-27}	163^{+43}_{-16}	$174.5^{+83.6}_{-24.3}$	$12.0^{+73.4}_{-6.2}$	$0.87^{+0.02}_{-0.31}$	113^{+70}_{-37}	3220	-2064	-23988
Pal 2	35.3	-108^{+5}_{-5}	11^{+22}_{-23}	108^{+8}_{-2}	$41.0^{+2.0}_{-2.2}$	$0.6^{+1.8}_{-0.4}$	$0.97^{+0.02}_{-0.08}$	42^{+70}_{-35}	506	373	-63896
NGC 1851	16.9	105^{+4}_{-4}	-1^{+5}_{-5}	133^{+4}_{-4}	$20.1^{+0.7}_{-0.2}$	$0.1^{+0.2}_{-0.0}$	$0.99^{+0.00}_{-0.02}$	92^{+9}_{-9}	232	-22	-94063
NGC 1904	19.0	46^{+8}_{-3}	12^{+12}_{-9}	47^{+9}_{-0}	$19.7^{+0.5}_{-0.9}$	$0.3^{+0.5}_{-0.1}$	$0.97^{+0.01}_{-0.05}$	60^{+27}_{-25}	218	211	-96192
NGC 2298	16.0	-92^{+6}_{-8}	-32^{+8}_{-10}	125^{+7}_{-8}	$18.0^{+0.7}_{-0.4}$	$1.2^{+0.5}_{-0.4}$	$0.87^{+0.04}_{-0.05}$	118^{+8}_{-5}	208	-500	-98716
NGC 2419	90.2	-5^{+10}_{-13}	47^{+30}_{-17}	75^{+31}_{-14}	$91.8^{+7.3}_{-6.1}$	$17.3^{+13.3}_{-5.5}$	$0.68^{+0.09}_{-0.18}$	52^{+14}_{-18}	1562	3907	-35896
Pyxis	41.5	-247^{+9}_{-5}	-29^{+21}_{-10}	311^{+13}_{-10}	$324.2^{+95.8}_{-90.9}$	$41.7^{+4.7}_{-12.8}$	$0.77^{+0.07}_{-0.01}$	98^{+2}_{-6}	7100	-1205	-15098
NGC 2808	11.3	-157^{+1}_{-2}	41^{+1}_{-7}	165^{+2}_{-1}	$14.4^{+0.7}_{-0.1}$	$1.0^{+0.0}_{-0.1}$	$0.87^{+0.02}_{-0.00}$	10^{+5}_{-0}	158	457	-111797
E 3	9.3	44^{+11}_{-16}	251^{+13}_{-18}	276^{+14}_{-18}	$13.1^{+1.9}_{-2.0}$	$9.2^{+0.4}_{-0.5}$	$0.18^{+0.06}_{-0.07}$	29^{+1}_{-1}	224	2240	-97684
Pal 3	95.9	-147^{+47}_{-70}	89^{+79}_{-62}	184^{+81}_{-60}	$173.4^{+77.4}_{-73.9}$	$76.3^{+29.1}_{-13.7}$	$0.39^{+0.38}_{-0.00}$	67^{+15}_{-14}	4524	6495	-20091
NGC 3201	9.1	-114^{+17}_{-18}	-301^{+9}_{-9}	355^{+12}_{-11}	$26.3^{+3.7}_{-3.0}$	$8.4^{+0.3}_{-0.3}$	$0.52^{+0.05}_{-0.05}$	152^{+1}_{-1}	372	-2728	-75483
Pal 4	111.4	-25^{+46}_{-67}	-33^{+63}_{-60}	70^{+72}_{-0}	$116.5^{+22.1}_{-8.5}$	$16.3^{+60.0}_{-1.6}$	$0.75^{+0.01}_{-0.05}$	103^{+7}_{-17}	2032	-1394	-31065
Crater	144.8	-101^{+110}_{-98}	-63^{+105}_{-270}	135^{+249}_{-0}	$156.1^{+97.5}_{-90.0}$	$117.4^{+42.6}_{-18.0}$	$0.14^{+0.73}_{-0.00}$	108^{+25}_{-26}	5082	-6104	-18859
NGC 4147	21.5	47^{+9}_{-8}	-3^{+12}_{-22}	136^{+5}_{-5}	$26.4^{+0.6}_{-1.9}$	$0.4^{+0.9}_{-0.0}$	$0.97^{+0.00}_{-0.07}$	93^{+20}_{-12}	314	-27	-81117
NGC 4372	7.3	16^{+11}_{-14}	133^{+6}_{-9}	150^{+6}_{-7}	$7.3^{+0.3}_{-0.2}$	$3.0^{+0.2}_{-0.3}$	$0.42^{+0.04}_{-0.02}$	28^{+3}_{-2}	98	962	-139570
Rup 106	18.5	-242^{+5}_{-8}	91^{+16}_{-15}	261^{+12}_{-7}	$37.9^{+5.6}_{-5.1}$	$4.7^{+0.9}_{-0.8}$	$0.78^{+0.03}_{-0.03}$	46^{+6}_{-4}	498	1640	-64986
NGC 4590	10.3	-169^{+7}_{-12}	293^{+6}_{-12}	339^{+4}_{-6}	$29.9^{+1.4}_{-2.4}$	$8.9^{+0.2}_{-0.4}$	$0.54^{+0.02}_{-0.02}$	41^{+2}_{-3}	428	2453	-70495
NGC 4833	7.2	105^{+12}_{-15}	40^{+12}_{-13}	120^{+12}_{-13}	$8.0^{+0.4}_{-0.3}$	$0.7^{+0.2}_{-0.3}$	$0.83^{+0.07}_{-0.04}$	36^{+13}_{-8}	86	286	-144428
NGC 5024	18.5	-95^{+7}_{-6}	141^{+8}_{-10}	184^{+7}_{-10}	$22.3^{+2.1}_{-2.0}$	$8.9^{+1.4}_{-1.4}$	$0.43^{+0.03}_{-0.03}$	74^{+2}_{-2}	332	797	-80241
NGC 5053	17.9	-89^{+5}_{-3}	134^{+5}_{-9}	164^{+4}_{-8}	$18.0^{+1.1}_{-0.6}$	$10.4^{+1.0}_{-1.1}$	$0.27^{+0.04}_{-0.03}$	76^{+1}_{-1}	300	727	-85221
NGC 5139	6.6	-70^{+7}_{-7}	-72^{+6}_{-7}	128^{+7}_{-9}	$7.4^{+0.1}_{-0.4}$	$1.1^{+0.3}_{-0.1}$	$0.73^{+0.02}_{-0.05}$	137^{+7}_{-5}	80	-462	-147850
NGC 5272	12.2	-38^{+7}_{-5}	143^{+10}_{-7}	200^{+8}_{-6}	$15.9^{+0.7}_{-0.9}$	$5.2^{+0.4}_{-0.3}$	$0.51^{+0.01}_{-0.03}$	57^{+1}_{-2}	212	994	-98226
NGC 5286	8.9	-220^{+4}_{-4}	-44^{+14}_{-15}	224^{+3}_{-1}	$13.7^{+1.2}_{-0.7}$	$0.8^{+0.4}_{-0.2}$	$0.89^{+0.02}_{-0.04}$	123^{+10}_{-10}	154	-375	-113332
NGC 5466	16.4	172^{+17}_{-22}	-141^{+29}_{-17}	317^{+8}_{-17}	$53.7^{+5.7}_{-10.4}$	$5.9^{+0.6}_{-1.1}$	$0.80^{+0.02}_{-0.02}$	108^{+2}_{-2}	750	-820	-52693
NGC 5634	21.1	-45^{+12}_{-16}	39^{+15}_{-5}	65^{+11}_{-5}	$21.6^{+1.1}_{-1.1}$	$2.1^{+0.9}_{-0.3}$	$0.82^{+0.02}_{-0.06}$	70^{+7}_{-3}	256	346	-89143
NGC 5694	29.3	-185^{+8}_{-13}	-44^{+18}_{-22}	252^{+12}_{-10}	$70.4^{+10.4}_{-7.8}$	$2.5^{+1.7}_{-1.0}$	$0.93^{+0.03}_{-0.04}$	136^{+10}_{-17}	992	-1019	-45290
IC 4499	15.6	-245^{+7}_{-4}	-75^{+9}_{-14}	263^{+4}_{-5}	$30.0^{+3.1}_{-2.7}$	$6.5^{+0.8}_{-0.4}$	$0.65^{+0.02}_{-0.05}$	113^{+4}_{-3}	406	-1066	-72235
NGC 5824	25.7	-41^{+17}_{-20}	105^{+13}_{-24}	215^{+11}_{-14}	$37.4^{+2.6}_{-4.3}$	$14.0^{+1.7}_{-3.6}$	$0.45^{+0.10}_{-0.05}$	58^{+4}_{-2}	598	2393	-59779
Pal 5	18.4	-54^{+5}_{-6}	160^{+39}_{-43}	169^{+37}_{-38}	$18.9^{+2.4}_{-0.6}$	$10.7^{+4.3}_{-3.6}$	$0.28^{+0.18}_{-0.13}$	66^{+4}_{-4}	308	1260	-83194
NGC 5897	7.3	88^{+13}_{-26}	97^{+14}_{-23}	159^{+8}_{-19}	$8.7^{+0.6}_{-0.4}$	$1.9^{+0.4}_{-0.5}$	$0.64^{+0.08}_{-0.05}$	61^{+5}_{-5}	106	362	-131771
NGC 5904	6.3	-290^{+17}_{-15}	126^{+11}_{-14}	365^{+13}_{-14}	$23.3^{+3.9}_{-3.3}$	$2.3^{+0.5}_{-0.3}$	$0.82^{+0.03}_{-0.03}$	72^{+3}_{-3}	286	402	-85576
NGC 5927	4.7	-39^{+20}_{-23}	233^{+6}_{-11}	236^{+6}_{-9}	$5.2^{+0.3}_{-0.2}$	$4.2^{+0.4}_{-0.5}$	$0.11^{+0.07}_{-0.05}$	9^{+1}_{-1}	82	1077	-148662
NGC 5946	5.8	35^{+6}_{-18}	25^{+6}_{-15}	116^{+9}_{-9}	$5.9^{+0.6}_{-0.2}$	$0.4^{+0.2}_{-0.2}$	$0.89^{+0.05}_{-0.05}$	77^{+8}_{-3}	66	141	-158006
ESO 224-8	12.6	-43^{+60}_{-14}	259^{+21}_{-22}	262^{+19}_{-21}	$17.0^{+3.0}_{-2.7}$	$11.9^{+0.9}_{-1.3}$	$0.18^{+0.09}_{-0.07}$	7^{+1}_{-1}	292	3245	-85205
NGC 5986	4.7	62^{+21}_{-33}	23^{+16}_{-15}	68^{+24}_{-32}	$5.2^{+0.6}_{-0.0}$	$0.2^{+0.5}_{-0.1}$	$0.93^{+0.05}_{-0.08}$	66^{+10}_{-14}	56	94	-168505
FSR 1716	4.8	87^{+47}_{-44}	228^{+21}_{-15}	281^{+24}_{-10}	$7.0^{+1.4}_{-0.7}$	$3.9^{+0.7}_{-0.7}$	$0.28^{+0.13}_{-0.07}$	31^{+2}_{-3}	106	1089	-137191
Pal 14	71.4	117^{+25}_{-18}	16^{+16}_{-41}	177^{+29}_{-17}	$133.9^{+31.3}_{-22.5}$	$2.2^{+5.2}_{-0.4}$	$0.97^{+0.00}_{-0.07}$	50^{+63}_{-0}	2202	794	-29458
BH 184	4.4	40^{+15}_{-21}	121^{+9}_{-11}	156^{+8}_{-9}	$4.7^{+0.4}_{-0.4}$	$1.7^{+0.2}_{-0.3}$	$0.47^{+0.06}_{-0.04}$	36^{+3}_{-3}	58	531	-168579
NGC 6093	3.7	33^{+12}_{-17}	16^{+9}_{-19}	71^{+9}_{-7}	$4.3^{+0.0}_{-0.9}$	$0.2^{+0.3}_{-0.1}$	$0.93^{+0.05}_{-0.03}$	83^{+8}_{-17}	44	25	-176933
NGC 6121	6.3	-52^{+2}_{-2}	10^{+18}_{-12}	54^{+7}_{-7}	$6.4^{+0.2}_{-0.1}$	$0.2^{+0.1}_{-0.1}$	$0.94^{+0.04}_{-0.03}$	21^{+82}_{-31}	68	60	-159021
NGC 6101	11.1	-12^{+29}_{-12}	-314^{+3}_{-2}	370^{+6}_{-4}	$44.2^{+4.1}_{-4.8}$	$10.9^{+0.4}_{-0.9}$	$0.61^{+0.02}_{-0.02}$	143^{+2}_{-2}	658	-3236	-56722
NGC 6144	2.7	-69^{+90}_{-93}	-196^{+66}_{-15}	213^{+7}_{-3}	$3.2^{+0.6}_{-0.0}$	$2.1^{+0.2}_{-0.3}$	$0.21^{+0.14}_{-0.01}$	114^{+8}_{-9}	40	-239	-172662
NGC 6139	3.5	-1^{+16}_{-16}	76^{+4}_{-8}	156^{+9}_{-9}	$3.6^{+0.3}_{-0.1}$	$1.1^{+0.2}_{-0.2}$	$0.54^{+0.07}_{-0.03}$	62^{+4}_{-3}	52	248	-176480
Terzan 3	2.5	-61^{+45}_{-51}	206^{+7}_{-22}	236^{+7}_{-8}	$3.2^{+0.4}_{-0.2}$	$2.2^{+0.1}_{-0.4}$	$0.18^{+0.13}_{-0.03}$	42^{+6}_{-4}	44	440	-175324

Table 1: continued.

Name	d_{GC} [kpc]	Π [km/s]	Θ [km/s]	V_{tot} [km/s]	apo [kpc]	peri [kpc]	ecc	incl. θ [deg]	T_r [Myr]	L_Z [kpc km/s]	E [km^2/s^2]
NGC 6171	3.5	-4^{+7}_{-3}	78^{+15}_{-8}	101^{+13}_{-6}	$3.8^{+0.3}_{-0.3}$	$0.6^{+0.3}_{-0.2}$	$0.72^{+0.08}_{-0.11}$	52^{+7}_{-4}	44	191	-178959
ESO 452-11	2.1	-24^{+11}_{-15}	-13^{+12}_{-11}	107^{+10}_{-2}	$2.9^{+0.4}_{-0.1}$	$0.0^{+0.1}_{-0.0}$	$0.97^{+0.01}_{-0.03}$	101^{+7}_{-10}	26	-16	-202684
NGC 6205	8.6	20^{+6}_{-4}	-26^{+5}_{-7}	87^{+5}_{-6}	$8.6^{+0.3}_{-0.2}$	$1.0^{+0.2}_{-0.1}$	$0.79^{+0.03}_{-0.03}$	105^{+4}_{-3}	100	-187	-134416
NGC 6229	29.9	30^{+11}_{-12}	6^{+8}_{-9}	59^{+8}_{-13}	$31.0^{+1.1}_{-1.0}$	$0.5^{+0.6}_{-0.1}$	$0.97^{+0.01}_{-0.04}$	77^{+26}_{-21}	376	135	-74434
NGC 6218	4.8	-9^{+3}_{-9}	135^{+6}_{-10}	158^{+6}_{-7}	$5.0^{+0.4}_{-0.1}$	$2.3^{+0.3}_{-0.2}$	$0.37^{+0.05}_{-0.02}$	37^{+2}_{-2}	64	581	-158135
FSR 1735	4.3	-102^{+17}_{-7}	-5^{+15}_{-21}	225^{+16}_{-12}	$5.3^{+0.6}_{-0.3}$	$1.0^{+0.5}_{-0.1}$	$0.69^{+0.03}_{-0.10}$	92^{+6}_{-4}	68	-22	-157538
NGC 6235	4.0	159^{+8}_{-5}	197^{+28}_{-40}	256^{+24}_{-30}	$6.2^{+1.2}_{-1.1}$	$2.7^{+0.4}_{-0.5}$	$0.39^{+0.05}_{-0.03}$	53^{+11}_{-7}	84	570	-145439
NGC 6254	4.8	-87^{+4}_{-7}	134^{+13}_{-16}	167^{+9}_{-10}	$5.2^{+0.2}_{-0.3}$	$2.1^{+0.3}_{-0.4}$	$0.42^{+0.06}_{-0.06}$	36^{+4}_{-1}	78	606	-157472
NGC 6256	2.9	-170^{+18}_{-0}	28^{+39}_{-18}	198^{+4}_{-11}	$4.4^{+0.9}_{-0.8}$	$0.1^{+0.3}_{-0.1}$	$0.94^{+0.04}_{-0.15}$	78^{+7}_{-14}	46	79	-181873
Pal 15	38.2	154^{+9}_{-13}	-5^{+26}_{-11}	162^{+9}_{-11}	$54.6^{+2.8}_{-4.4}$	$1.2^{+3.0}_{-0.3}$	$0.96^{+0.01}_{-0.11}$	98^{+18}_{-35}	726	-165	-53233
NGC 6266	2.0	42^{+17}_{-15}	122^{+10}_{-18}	146^{+6}_{-11}	$2.5^{+0.5}_{-0.4}$	$0.6^{+0.3}_{-0.1}$	$0.62^{+0.04}_{-0.10}$	32^{+4}_{-4}	32	215	-205537
NGC 6273	1.6	-98^{+67}_{-143}	-240^{+218}_{-34}	315^{+8}_{-4}	$3.8^{+0.6}_{-0.3}$	$1.0^{+0.1}_{-0.1}$	$0.59^{+0.11}_{-0.08}$	109^{+10}_{-18}	48	-144	-172941
NGC 6284	7.3	14^{+2}_{-2}	-2^{+7}_{-19}	113^{+12}_{-6}	$7.5^{+0.9}_{-0.9}$	$0.7^{+0.3}_{-0.2}$	$0.83^{+0.04}_{-0.06}$	91^{+10}_{-4}	90	-16	-142332
NGC 6287	2.0	-301^{+264}_{-107}	-64^{+40}_{-80}	318^{+5}_{-4}	$5.3^{+0.6}_{-0.5}$	$0.8^{+0.1}_{-0.1}$	$0.75^{+0.04}_{-0.02}$	95^{+3}_{-3}	66	-60	-159009
NGC 6293	1.8	-152^{+52}_{-33}	-80^{+115}_{-36}	233^{+7}_{-10}	$3.6^{+0.4}_{-1.0}$	$0.2^{+0.2}_{-0.1}$	$0.91^{+0.08}_{-0.17}$	131^{+7}_{-39}	38	-93	-191358
NGC 6304	2.5	79^{+5}_{-10}	191^{+7}_{-6}	219^{+5}_{-6}	$3.3^{+0.4}_{-0.6}$	$1.8^{+0.2}_{-0.4}$	$0.29^{+0.04}_{-0.02}$	20^{+2}_{-2}	52	474	-183132
NGC 6316	2.4	103^{+9}_{-7}	51^{+26}_{-33}	143^{+16}_{-11}	$3.0^{+0.5}_{-0.6}$	$0.4^{+0.1}_{-0.3}$	$0.77^{+0.18}_{-0.03}$	40^{+31}_{-16}	36	106	-197316
NGC 6341	9.8	53^{+6}_{-4}	13^{+9}_{-5}	109^{+12}_{-13}	$10.7^{+0.3}_{-0.3}$	$0.3^{+0.2}_{-0.1}$	$0.94^{+0.02}_{-0.04}$	79^{+4}_{-9}	124	108	-125312
NGC 6325	1.3	-81^{+29}_{-48}	-181^{+187}_{-63}	214^{+17}_{-19}	$1.3^{+0.4}_{-0.1}$	$1.1^{+0.2}_{-0.3}$	$0.12^{+0.16}_{-0.00}$	114^{+13}_{-25}	18	-107	-212097
NGC 6333	1.8	-89^{+122}_{-118}	346^{+6}_{-48}	364^{+5}_{-3}	$6.4^{+0.8}_{-0.2}$	$1.0^{+0.2}_{-0.1}$	$0.74^{+0.04}_{-0.03}$	59^{+2}_{-6}	74	327	-151409
NGC 6342	1.6	-25^{+70}_{-89}	164^{+13}_{-66}	168^{+6}_{-4}	$1.7^{+0.7}_{-0.3}$	$0.9^{+0.2}_{-0.4}$	$0.31^{+0.29}_{-0.12}$	64^{+6}_{-3}	24	117	-207010
NGC 6356	7.2	47^{+5}_{-9}	107^{+25}_{-12}	160^{+17}_{-7}	$7.9^{+1.3}_{-1.1}$	$2.5^{+1.0}_{-0.5}$	$0.52^{+0.06}_{-0.10}$	43^{+3}_{-4}	104	713	-136303
NGC 6355	1.2	-207^{+70}_{-47}	-110^{+108}_{-54}	275^{+8}_{-7}	$2.2^{+1.1}_{-0.5}$	$0.6^{+0.2}_{-0.2}$	$0.56^{+0.17}_{-0.10}$	106^{+8}_{-10}	28	-95	-199192
NGC 6352	3.6	42^{+18}_{-13}	226^{+5}_{-10}	230^{+4}_{-10}	$4.1^{+0.6}_{-0.3}$	$3.2^{+0.2}_{-0.3}$	$0.13^{+0.05}_{-0.03}$	12^{+1}_{-1}	68	794	-163864
IC 1257	17.6	-45^{+7}_{-12}	-50^{+12}_{-18}	70^{+12}_{-0}	$18.1^{+1.1}_{-0.8}$	$1.8^{+0.8}_{-0.4}$	$0.82^{+0.04}_{-0.08}$	158^{+4}_{-11}	208	-817	-98556
Terzan 2	1.0	-120^{+62}_{-23}	-47^{+13}_{-48}	136^{+3}_{-2}	$1.2^{+0.3}_{-0.4}$	$0.1^{+0.1}_{-0.0}$	$0.86^{+0.05}_{-0.19}$	161^{+3}_{-19}	14	-44	-242360
NGC 6366	5.3	94^{+3}_{-3}	134^{+2}_{-6}	175^{+2}_{-5}	$5.8^{+0.2}_{-0.2}$	$2.2^{+0.1}_{-0.2}$	$0.45^{+0.03}_{-0.00}$	32^{+2}_{-1}	74	699	-153378
Terzan 4	1.2	15^{+8}_{-39}	75^{+18}_{-13}	124^{+14}_{-8}	$1.3^{+0.2}_{-0.4}$	$0.2^{+0.1}_{-0.1}$	$0.68^{+0.03}_{-0.10}$	52^{+7}_{-6}	14	92	-234494
BH 229	0.5	7^{+46}_{-39}	-55^{+48}_{-0}	292^{+14}_{-22}	$0.8^{+1.1}_{-0.1}$	$0.3^{+0.4}_{-0.2}$	$0.49^{+0.32}_{-0.18}$	100^{+0}_{-9}	10	-21	-249808
FSR 1758	3.7	60^{+30}_{-60}	-347^{+8}_{-6}	405^{+8}_{-8}	$14.3^{+2.3}_{-2.1}$	$3.7^{+0.4}_{-0.5}$	$0.59^{+0.03}_{-0.02}$	148^{+2}_{-2}	178	-1275	-106508
NGC 6362	5.2	17^{+14}_{-28}	124^{+11}_{-6}	160^{+11}_{-4}	$5.3^{+0.2}_{-0.4}$	$2.5^{+0.2}_{-0.3}$	$0.37^{+0.04}_{-0.04}$	45^{+2}_{-4}	70	583	-153468
Liller 1	0.8	107^{+25}_{-57}	-56^{+61}_{-43}	123^{+28}_{-31}	$0.8^{+0.2}_{-0.1}$	$0.1^{+0.2}_{-0.1}$	$0.81^{+0.13}_{-0.16}$	155^{+16}_{-74}	8	-42	-261395
NGC6380	3.1	-62^{+5}_{-14}	-35^{+16}_{-9}	72^{+14}_{-7}	$3.4^{+0.2}_{-0.6}$	$0.2^{+0.1}_{-0.1}$	$0.89^{+0.05}_{-0.07}$	168^{+11}_{-26}	40	-105	-194646
Terzan 1	1.6	-73^{+3}_{-5}	63^{+10}_{-20}	96^{+8}_{-11}	$1.8^{+0.5}_{-0.6}$	$0.2^{+0.1}_{-0.1}$	$0.79^{+0.06}_{-0.04}$	11^{+10}_{-6}	22	102	-224803
Pismis 26	1.4	-112^{+111}_{-58}	204^{+32}_{-55}	307^{+9}_{-8}	$3.2^{+0.8}_{-0.1}$	$0.9^{+0.7}_{-0.4}$	$0.56^{+0.17}_{-0.20}$	41^{+9}_{-2}	44	271	-186876
NGC 6388	3.0	-66^{+24}_{-19}	-94^{+6}_{-12}	116^{+6}_{-7}	$3.5^{+0.4}_{-0.2}$	$0.7^{+0.4}_{-0.2}$	$0.69^{+0.07}_{-0.13}$	148^{+8}_{-9}	46	-257	-190150
NGC 6402	4.0	-20^{+23}_{-21}	48^{+12}_{-7}	57^{+16}_{-7}	$4.8^{+0.2}_{-0.5}$	$0.3^{+0.2}_{-0.0}$	$0.88^{+0.00}_{-0.08}$	47^{+6}_{-10}	52	158	-176457
NGC 6401	2.5	-30^{+27}_{-18}	-254^{+4}_{-4}	302^{+8}_{-4}	$4.5^{+0.8}_{-0.7}$	$2.4^{+0.6}_{-0.6}$	$0.31^{+0.07}_{-0.03}$	143^{+2}_{-3}	62	-595	-161761
NGC 6397	6.3	35^{+7}_{-6}	127^{+11}_{-9}	179^{+9}_{-4}	$6.5^{+0.1}_{-0.2}$	$2.8^{+0.3}_{-0.2}$	$0.40^{+0.01}_{-0.04}$	43^{+2}_{-4}	86	796	-144538
Pal 6	2.5	-191^{+2}_{-3}	21^{+16}_{-14}	246^{+6}_{-8}	$4.5^{+0.4}_{-0.8}$	$0.0^{+1.1}_{-0.0}$	$0.96^{+0.01}_{-0.03}$	83^{+4}_{-6}	44	52	-179351
NGC 6426	14.3	-112^{+27}_{-16}	93^{+7}_{-20}	148^{+11}_{-25}	$16.6^{+1.1}_{-0.7}$	$3.2^{+0.5}_{-0.9}$	$0.67^{+0.08}_{-0.03}$	27^{+4}_{-4}	202	1216	-100666
Djorg 1	1.2	-252^{+271}_{-102}	315^{+49}_{-51}	404^{+12}_{-9}	$5.9^{+1.6}_{-1.6}$	$0.8^{+0.1}_{-0.2}$	$0.76^{+0.05}_{-0.06}$	21^{+13}_{-7}	66	351	-161437
Terzan 5	1.5	84^{+11}_{-6}	70^{+13}_{-23}	114^{+9}_{-7}	$1.7^{+0.5}_{-0.6}$	$0.2^{+0.1}_{-0.1}$	$0.78^{+0.04}_{-0.05}$	33^{+18}_{-7}	20	104	-226313
NGC 6440	1.3	91^{+18}_{-36}	-42^{+54}_{-34}	107^{+10}_{-8}	$1.4^{+0.4}_{-0.0}$	$0.2^{+0.1}_{-0.1}$	$0.78^{+0.15}_{-0.07}$	116^{+21}_{-34}	14	-49	-231796
NGC 6441	3.6	16^{+15}_{-8}	66^{+18}_{-19}	71^{+20}_{-16}	$3.6^{+0.7}_{-0.6}$	$0.8^{+0.2}_{-0.2}$	$0.66^{+0.09}_{-0.07}$	21^{+11}_{-6}	42	228	-186312
Terzan 6	1.5	-138^{+7}_{-3}	-51^{+21}_{-32}	153^{+9}_{-3}	$2.0^{+0.2}_{-0.6}$	$0.1^{+0.1}_{-0.1}$	$0.86^{+0.05}_{-0.11}$	157^{+17}_{-26}	22	-77	-220185
NGC 6453	3.4	-105^{+9}_{-6}	38^{+30}_{-15}	194^{+19}_{-5}	$3.9^{+0.8}_{-0.6}$	$0.9^{+0.5}_{-0.4}$	$0.61^{+0.04}_{-0.14}$	78^{+5}_{-8}	54	129	-172906
NGC 6496	4.0	-37^{+76}_{-63}	320^{+24}_{-41}	328^{+26}_{-28}	$9.1^{+2.1}_{-1.6}$	$3.7^{+0.4}_{-0.6}$	$0.42^{+0.10}_{-0.07}$	32^{+5}_{-3}	120	1111	-126509
Terzan 9	1.3	-50^{+8}_{-7}	22^{+18}_{-14}	76^{+7}_{-2}	$1.4^{+0.6}_{-0.4}$	$0.1^{+0.1}_{-0.0}$	$0.92^{+0.03}_{-0.08}$	70^{+12}_{-13}	16	29	-236057
Djorg 2	2.0	161^{+9}_{-6}	155^{+6}_{-11}	228^{+3}_{-4}	$3.2^{+0.6}_{-0.7}$	$0.9^{+0.3}_{-0.3}$	$0.57^{+0.06}_{-0.04}$	11^{+1}_{-1}	42	316	-192751
NGC 6517	4.0	55^{+8}_{-17}	33^{+10}_{-12}	73^{+5}_{-11}	$4.6^{+0.4}_{-0.4}$	$0.2^{+0.1}_{-0.1}$	$0.91^{+0.03}_{-0.04}$	58^{+10}_{-10}	50	127	-179281
Terzan 10	2.2	231^{+20}_{-52}	87^{+64}_{-22}	343^{+20}_{-13}	$5.9^{+1.4}_{-1.8}$	$0.7^{+0.3}_{-0.1}$	$0.79^{+0.04}_{-0.11}$	72^{+4}_{-10}	76	193	-155422

Table 1: continued.

Name	d_{GC} [kpc]	Π [km/s]	Θ [km/s]	V_{tot} [km/s]	apo [kpc]	peri [kpc]	ecc	incl. θ [deg]	T_r [Myr]	L_Z [kpc km/s]	E [km^2/s^2]
NGC 6522	0.8	34^{+25}_{-15}	92^{+23}_{-57}	213^{+17}_{-9}	$1.2^{+0.5}_{-0.3}$	$0.2^{+0.3}_{-0.2}$	$0.67^{+0.14}_{-0.15}$	63^{+16}_{-6}	16	58	-238519
NGC 6535	4.0	93^{+9}_{-10}	-83^{+13}_{-8}	133^{+2}_{-6}	$4.6^{+0.4}_{-0.3}$	$1.0^{+0.1}_{-0.2}$	$0.64^{+0.06}_{-0.03}$	160^{+1}_{-3}	56	-320	-173024
NGC 6528	0.7	-197^{+300}_{-67}	113^{+31}_{-67}	229^{+2}_{-2}	$1.0^{+0.9}_{-0.2}$	$0.3^{+0.0}_{-0.2}$	$0.60^{+0.33}_{-0.14}$	70^{+7}_{-5}	14	51	-241883
NGC 6539	3.1	1^{+28}_{-9}	118^{+5}_{-3}	208^{+14}_{-9}	$3.4^{+0.3}_{-0.2}$	$1.9^{+0.2}_{-0.3}$	$0.30^{+0.08}_{-0.03}$	56^{+1}_{-2}	56	347	-174387
NGC 6540	3.0	13^{+3}_{-2}	148^{+9}_{-7}	159^{+8}_{-5}	$3.1^{+0.4}_{-0.4}$	$1.6^{+0.3}_{-0.2}$	$0.32^{+0.04}_{-0.04}$	22^{+2}_{-1}	48	448	-187517
NGC 6544	5.3	6^{+2}_{-2}	6^{+14}_{-10}	91^{+7}_{-7}	$5.6^{+0.2}_{-0.1}$	$0.1^{+0.2}_{-0.0}$	$0.98^{+0.00}_{-0.06}$	86^{+7}_{-9}	52	31	-166630
NGC 6541	2.3	123^{+33}_{-62}	192^{+25}_{-20}	254^{+11}_{-6}	$3.8^{+0.6}_{-0.6}$	$1.3^{+0.2}_{-0.1}$	$0.50^{+0.08}_{-0.10}$	40^{+6}_{-4}	50	334	-174968
ESO 280-06	13.8	31^{+5}_{-10}	16^{+10}_{-25}	91^{+8}_{-11}	$14.2^{+1.1}_{-1.3}$	$0.9^{+0.5}_{-0.4}$	$0.88^{+0.05}_{-0.05}$	77^{+20}_{-7}	164	210	-109791
NGC 6553	2.4	45^{+15}_{-12}	245^{+2}_{-4}	250^{+2}_{-3}	$3.3^{+0.3}_{-0.4}$	$2.3^{+0.4}_{-0.5}$	$0.19^{+0.04}_{-0.04}$	7^{+2}_{-1}	52	588	-179839
NGC 6558	1.2	187^{+60}_{-94}	93^{+36}_{-60}	209^{+4}_{-4}	$1.7^{+0.4}_{-0.6}$	$0.3^{+0.2}_{-0.0}$	$0.72^{+0.08}_{-0.29}$	63^{+15}_{-8}	20	87	-217130
Pal 7	3.9	-74^{+12}_{-9}	270^{+7}_{-4}	281^{+7}_{-4}	$6.0^{+0.6}_{-0.4}$	$3.5^{+0.3}_{-0.1}$	$0.26^{+0.03}_{-0.02}$	11^{+1}_{-1}	86	1042	-147032
Terzan 12	3.6	-94^{+5}_{-4}	172^{+8}_{-6}	219^{+6}_{-4}	$4.4^{+0.4}_{-0.5}$	$2.2^{+0.2}_{-0.3}$	$0.33^{+0.04}_{-0.02}$	28^{+2}_{-2}	62	625	-167749
NGC 6569	2.8	-40^{+2}_{-4}	174^{+18}_{-26}	180^{+18}_{-25}	$3.0^{+0.6}_{-0.7}$	$1.9^{+0.3}_{-0.7}$	$0.23^{+0.17}_{-0.05}$	26^{+12}_{-5}	56	440	-182361
ESO 456-78	2.0	71^{+10}_{-10}	199^{+5}_{-4}	252^{+7}_{-6}	$2.9^{+0.6}_{-0.2}$	$1.4^{+0.5}_{-0.3}$	$0.34^{+0.06}_{-0.07}$	34^{+2}_{-4}	52	373	-186632
NGC 6584	6.8	197^{+7}_{-30}	98^{+22}_{-34}	324^{+11}_{-22}	$18.0^{+2.1}_{-2.8}$	$1.7^{+0.7}_{-0.6}$	$0.83^{+0.05}_{-0.06}$	52^{+12}_{-3}	212	556	-98089
NGC 6624	1.2	-29^{+48}_{-24}	60^{+14}_{-18}	136^{+7}_{-4}	$1.5^{+0.3}_{-0.0}$	$0.2^{+0.1}_{-0.2}$	$0.78^{+0.18}_{-0.05}$	73^{+3}_{-6}	20	37	-226410
NGC 6626	3.0	-28^{+2}_{-4}	57^{+9}_{-12}	113^{+8}_{-5}	$3.1^{+0.5}_{-0.1}$	$0.5^{+0.1}_{-0.2}$	$0.75^{+0.10}_{-0.04}$	60^{+6}_{-4}	42	169	-193067
NGC 6638	2.0	68^{+16}_{-12}	14^{+13}_{-21}	74^{+14}_{-7}	$2.4^{+0.5}_{-0.1}$	$0.1^{+0.0}_{-0.0}$	$0.95^{+0.03}_{-0.03}$	80^{+16}_{-9}	20	22	-212068
NGC 6637	1.6	35^{+27}_{-111}	91^{+6}_{-81}	129^{+8}_{-5}	$2.2^{+0.2}_{-0.4}$	$0.2^{+0.0}_{-0.1}$	$0.87^{+0.11}_{-0.01}$	77^{+17}_{-5}	22	40	-212500
NGC 6642	1.7	112^{+6}_{-22}	25^{+32}_{-51}	125^{+8}_{-11}	$2.2^{+0.3}_{-0.1}$	$0.1^{+0.2}_{-0.0}$	$0.94^{+0.02}_{-0.11}$	46^{+78}_{-17}	24	36	-215457
NGC 6652	2.5	-54^{+6}_{-4}	28^{+7}_{-18}	186^{+11}_{-16}	$4.2^{+0.2}_{-0.3}$	$0.1^{+0.1}_{-0.1}$	$0.96^{+0.03}_{-0.05}$	76^{+9}_{-5}	38	42	-183595
NGC 6656	5.2	176^{+3}_{-2}	201^{+2}_{-2}	303^{+6}_{-5}	$9.8^{+0.7}_{-0.5}$	$3.1^{+0.2}_{-0.1}$	$0.53^{+0.01}_{-0.01}$	33^{+2}_{-2}	126	1044	-125471
Pal 8	5.3	-21^{+13}_{-25}	117^{+23}_{-15}	122^{+27}_{-15}	$5.6^{+0.3}_{-0.6}$	$1.8^{+0.6}_{-0.4}$	$0.51^{+0.06}_{-0.11}$	23^{+3}_{-2}	72	593	-160020
NGC 6681	2.0	221^{+34}_{-166}	55^{+135}_{-44}	287^{+4}_{-3}	$4.5^{+0.3}_{-0.4}$	$0.7^{+0.5}_{-0.1}$	$0.74^{+0.10}_{-0.15}$	84^{+8}_{-9}	52	36	-167768
NGC 6712	3.6	146^{+6}_{-7}	26^{+9}_{-17}	208^{+7}_{-10}	$5.5^{+0.3}_{-0.2}$	$0.2^{+0.1}_{-0.1}$	$0.93^{+0.04}_{-0.02}$	78^{+7}_{-4}	56	93	-168544
NGC 6715	18.6	232^{+6}_{-8}	49^{+25}_{-22}	317^{+21}_{-11}	$56.4^{+24.2}_{-10.1}$	$14.8^{+1.8}_{-1.0}$	$0.58^{+0.07}_{-0.03}$	81^{+4}_{-4}	906	850	-48159
NGC 6717	2.5	-10^{+31}_{-13}	116^{+9}_{-9}	119^{+9}_{-7}	$2.8^{+0.4}_{-0.4}$	$0.7^{+0.2}_{-0.1}$	$0.59^{+0.06}_{-0.09}$	32^{+7}_{-4}	36	251	-195762
NGC 6723	2.6	100^{+6}_{-192}	-178^{+353}_{-3}	208^{+5}_{-3}	$3.1^{+0.4}_{-0.0}$	$1.8^{+0.2}_{-0.0}$	$0.26^{+0.03}_{-0.03}$	90^{+8}_{-12}	40	-2	-175356
NGC 6749	5.0	-23^{+17}_{-10}	110^{+10}_{-8}	112^{+10}_{-8}	$5.1^{+0.4}_{-0.2}$	$1.6^{+0.2}_{-0.2}$	$0.53^{+0.05}_{-0.05}$	3^{+1}_{-0}	62	556	-167068
NGC 6752	5.5	-23^{+7}_{-2}	179^{+3}_{-6}	190^{+3}_{-6}	$5.7^{+0.3}_{-0.3}$	$3.6^{+0.2}_{-0.2}$	$0.23^{+0.02}_{-0.02}$	24^{+1}_{-1}	82	931	-147164
NGC 6760	5.0	92^{+10}_{-9}	147^{+7}_{-8}	174^{+7}_{-7}	$5.6^{+0.3}_{-0.3}$	$2.2^{+0.2}_{-0.2}$	$0.44^{+0.04}_{-0.03}$	6^{+1}_{-0}	72	724	-158732
NGC 6779	9.3	155^{+3}_{-2}	-15^{+6}_{-9}	185^{+6}_{-4}	$12.4^{+0.4}_{-0.6}$	$0.3^{+0.2}_{-0.2}$	$0.96^{+0.01}_{-0.03}$	101^{+7}_{-5}	134	-135	-119696
Terzan 7	15.3	260^{+6}_{-6}	25^{+17}_{-11}	320^{+11}_{-11}	$42.9^{+7.7}_{-8.3}$	$12.8^{+0.6}_{-1.1}$	$0.54^{+0.05}_{-0.05}$	86^{+2}_{-3}	668	335	-56545
Pal 10	6.6	-56^{+15}_{-5}	186^{+8}_{-14}	195^{+7}_{-4}	$7.0^{+0.3}_{-0.3}$	$4.0^{+0.4}_{-0.3}$	$0.27^{+0.04}_{-0.03}$	8^{+1}_{-1}	100	1234	-138495
Arp 2	21.2	243^{+7}_{-8}	68^{+20}_{-11}	311^{+10}_{-15}	$65.1^{+21.7}_{-13.5}$	$17.8^{+1.7}_{-1.6}$	$0.57^{+0.06}_{-0.04}$	78^{+2}_{-4}	1094	1256	-43628
NGC 6809	4.1	-199^{+5}_{-7}	76^{+15}_{-19}	220^{+5}_{-3}	$5.7^{+0.4}_{-0.5}$	$1.2^{+0.3}_{-0.3}$	$0.66^{+0.06}_{-0.07}$	67^{+6}_{-3}	76	266	-154417
Terzan 8	19.1	269^{+5}_{-5}	37^{+16}_{-23}	315^{+12}_{-7}	$58.5^{+13.5}_{-6.8}$	$16.0^{+0.8}_{-0.8}$	$0.57^{+0.06}_{-0.03}$	84^{+4}_{-3}	958	584	-46785
Pal 11	8.1	-16^{+28}_{-20}	139^{+12}_{-10}	140^{+14}_{-9}	$8.2^{+0.7}_{-0.4}$	$3.5^{+0.6}_{-0.4}$	$0.40^{+0.05}_{-0.04}$	27^{+3}_{-2}	108	1013	-132057
NGC 6838	7.0	39^{+5}_{-11}	204^{+5}_{-4}	212^{+4}_{-4}	$7.3^{+0.2}_{-0.2}$	$5.0^{+0.3}_{-0.2}$	$0.18^{+0.02}_{-0.03}$	12^{+1}_{-1}	112	1423	-132307
NGC 6864	14.6	-99^{+14}_{-6}	18^{+10}_{-25}	111^{+7}_{-14}	$16.4^{+1.3}_{-0.4}$	$0.5^{+0.6}_{-0.5}$	$0.94^{+0.06}_{-0.05}$	61^{+41}_{-9}	186	209	-103615
NGC 6934	12.7	-289^{+20}_{-18}	103^{+20}_{-30}	330^{+15}_{-17}	$40.9^{+7.8}_{-5.8}$	$2.5^{+0.6}_{-0.8}$	$0.88^{+0.04}_{-0.03}$	23^{+5}_{-2}	520	1204	-63341
NGC 6981	12.8	-154^{+10}_{-13}	-4^{+14}_{-25}	230^{+10}_{-7}	$22.3^{+2.1}_{-1.3}$	$0.3^{+0.3}_{-0.1}$	$0.97^{+0.01}_{-0.03}$	108^{+25}_{-36}	252	-35	-89722
NGC 7006	38.5	-140^{+6}_{-8}	-33^{+17}_{-7}	168^{+9}_{-12}	$56.3^{+2.3}_{-4.5}$	$2.9^{+0.7}_{-1.5}$	$0.90^{+0.05}_{-0.02}$	133^{+13}_{-13}	760	-1170	-52073
NGC 7078	10.6	8^{+11}_{-12}	118^{+8}_{-11}	122^{+9}_{-10}	$10.6^{+0.6}_{-0.5}$	$3.5^{+0.4}_{-0.5}$	$0.50^{+0.05}_{-0.04}$	28^{+3}_{-1}	140	1119	-119947
NGC 7089	10.4	170^{+5}_{-6}	-18^{+15}_{-15}	243^{+8}_{-8}	$18.8^{+1.7}_{-1.0}$	$0.6^{+0.2}_{-0.3}$	$0.94^{+0.03}_{-0.02}$	119^{+12}_{-20}	214	-147	-97640
NGC 7099	7.2	-32^{+14}_{-9}	-55^{+16}_{-12}	126^{+8}_{-9}	$8.2^{+0.6}_{-0.5}$	$1.0^{+0.3}_{-0.3}$	$0.78^{+0.06}_{-0.06}$	119^{+6}_{-6}	94	-234	-137480
Pal 12	15.7	146^{+22}_{-37}	304^{+22}_{-24}	356^{+12}_{-17}	$72.0^{+18.9}_{-16.0}$	$15.5^{+1.0}_{-0.9}$	$0.65^{+0.05}_{-0.08}$	67^{+2}_{-2}	1178	2142	-41826
Pal 13	27.0	268^{+6}_{-11}	-78^{+21}_{-17}	289^{+9}_{-6}	$87.1^{+8.6}_{-13.4}$	$8.3^{+0.9}_{-0.9}$	$0.83^{+0.03}_{-0.02}$	115^{+8}_{-6}	1346	-1586	-38661
NGC 7492	25.4	-87^{+16}_{-22}	-13^{+9}_{-7}	108^{+19}_{-10}	$28.2^{+2.5}_{-2.3}$	$3.1^{+1.4}_{-1.0}$	$0.80^{+0.06}_{-0.07}$	95^{+6}_{-5}	352	-120	-77041

9

Table 2: Globular clusters with modified classification.

Name	GS	GS(m)	Name	GS	GS(m)	Name	GS	GS(m)
E 3	H99	D	NGC 6254	LE	D	NGC 6553	B	D
NGC 5466	Seq	GE	NGC 6304	B	D	NGC 6569	B	D
NGC 5634	H99	GE	Liller 1	XXX	B	ESO 456-78	B	D
NGC 5694	HE	GE	NGC 6388	B	Seq	NGC 6584	HE	GE
NGC 5824	Sgr	H99	NGC 6401	LE	Seq	NGC 6712	LE	GE
NGC 5904	H99	GE	NGC 6426	HE	H99	NGC 6934	HE	GE
Pal 14	HE	GE	NGC 6539	B	D	NGC 6981	H99	GE
NGC 6144	LE	Seq	NGC 6540	B	D	NGC 7006	Seq	GE
NGC 6235	GE	D	NGC 6544	LE	GE	Pal 13	Seq	GE

The separation of globular clusters into subsystems of the bulge/bar, thick disk, and halo was performed by us in work Bajkova et al. (2020) using a criterion based on the bimodal distribution of globular clusters over parameter L_Z/ecc. The composition of the bulge/bar and thick disk reflects these results. In the redistribution of the remaining globular clusters between the halo subsystems (GE, Seq, Sgr, H99), we took into account the parameters of the orbits. For example, globular clusters with strong radially elongated orbits were assigned to GE. The rest of the rearrangement also took into account the proximity of the orbital shapes.

In Fig. 3 the "L_Z– Energy", "L_Z/ecc– Energy" and "Radial velocity – Rotational velocity" diagrams are presented. These diagrams are given both for classification of GCs by Massari et al. (2019) and for the modified one for comparison. As you can see from Fig. 2, the modified classification looks like a more correct one from the point of view of a greater similarity of the orbits of globular clusters included in their subsystem. From a comparison of the diagrams "L_Z – Energy", "L_Z/ecc – Energy" and "Radial velocity – Rotational velocity", it can also be concluded that the modified classification is more organic.

6   Conclusions

For the first time since the emergence of the Gaia Data Release 2, a catalog of orbits for 152 galactic globular clusters, which form an almost complete known population, is presented.

The main orbital parameters of globular clusters are determined. The astrometric data catalog compiled by Vasiliev (2019) was used as data for calculating the initial 6d phase space (heliocentric positions and velocities of globular clusters) needed for orbit construction. The orbits were integrated for 5 Gyr backward.

For integrating the orbits, we used a recently obtained by Bajkova & Bobylev (2016) the best-fit model of an axisymmetric Galactic potential with a dark halo in the form of NFW (Navarro et al., 1997) using data on circular velocities of Galactic objects in a wide range of galactocentric distances (data on HI region, masers, and catalog of Bhattacharjee et al. (2014)).

Based on the analysis of the obtained orbits and their properties, we have formed a modified composition of the subsystems of globular clusters, slightly different from the composition presented in Massari et al. (2019). This modification affected 27 GCs. The modified classification looks like a more correct one from the point of view of a greater similarity of the orbits of globular clusters included in their subsystem.
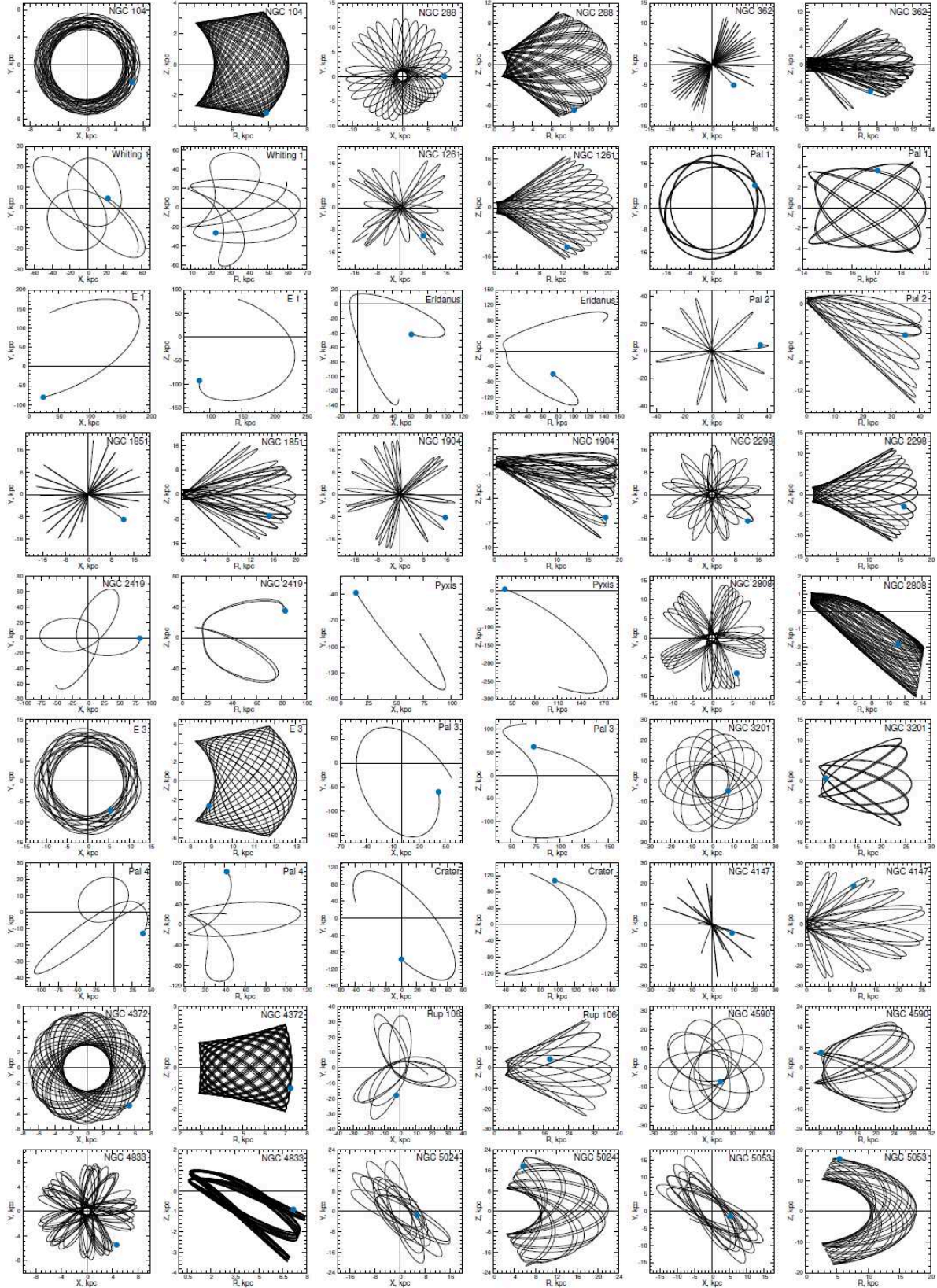
Figure 2: Orbits of the GCs obtained by integrating for 5 Gyr backward. (X,Y) and (R,Z) projections are given. The blue filled circle indicates the beginning of the orbit.
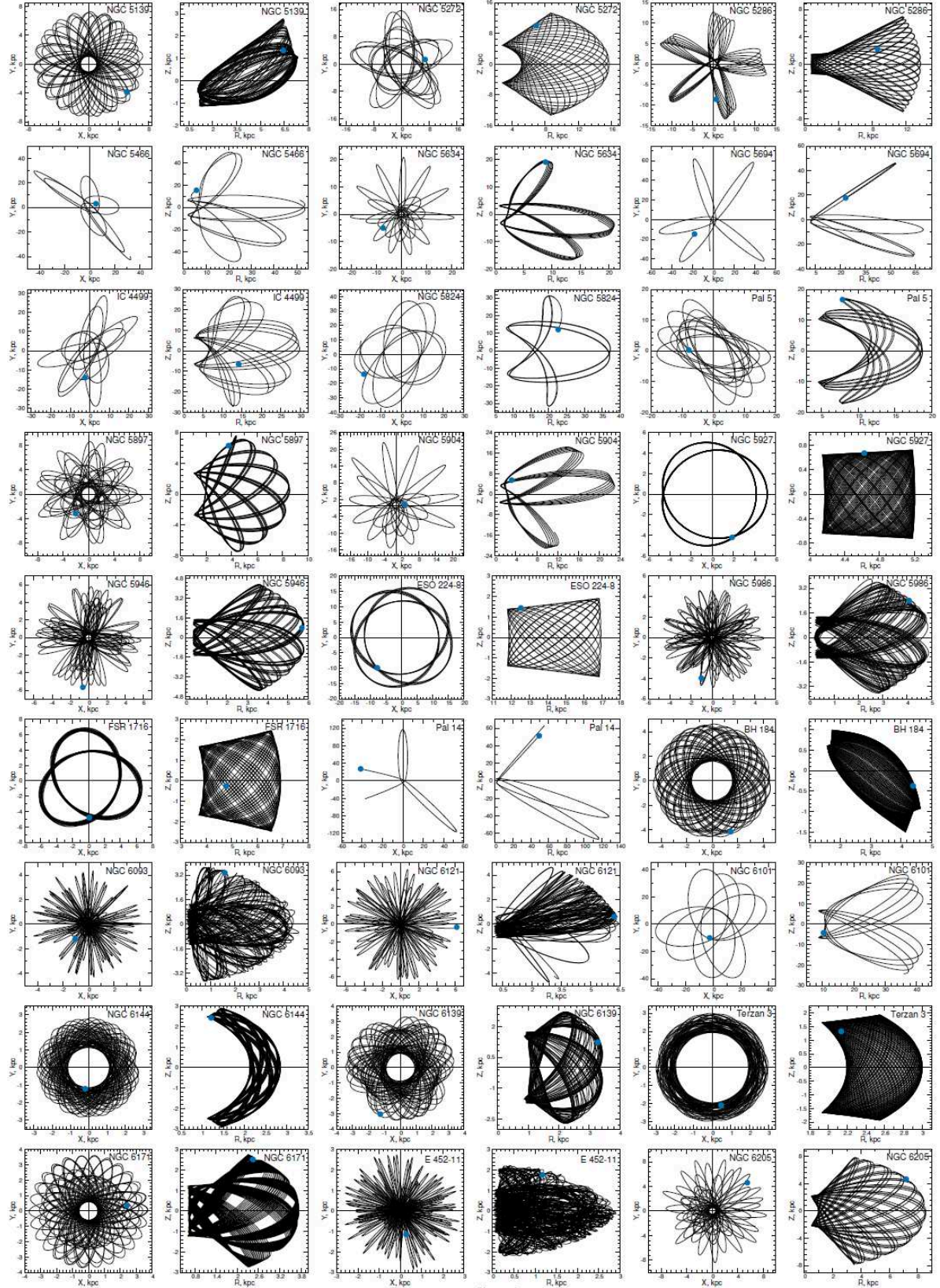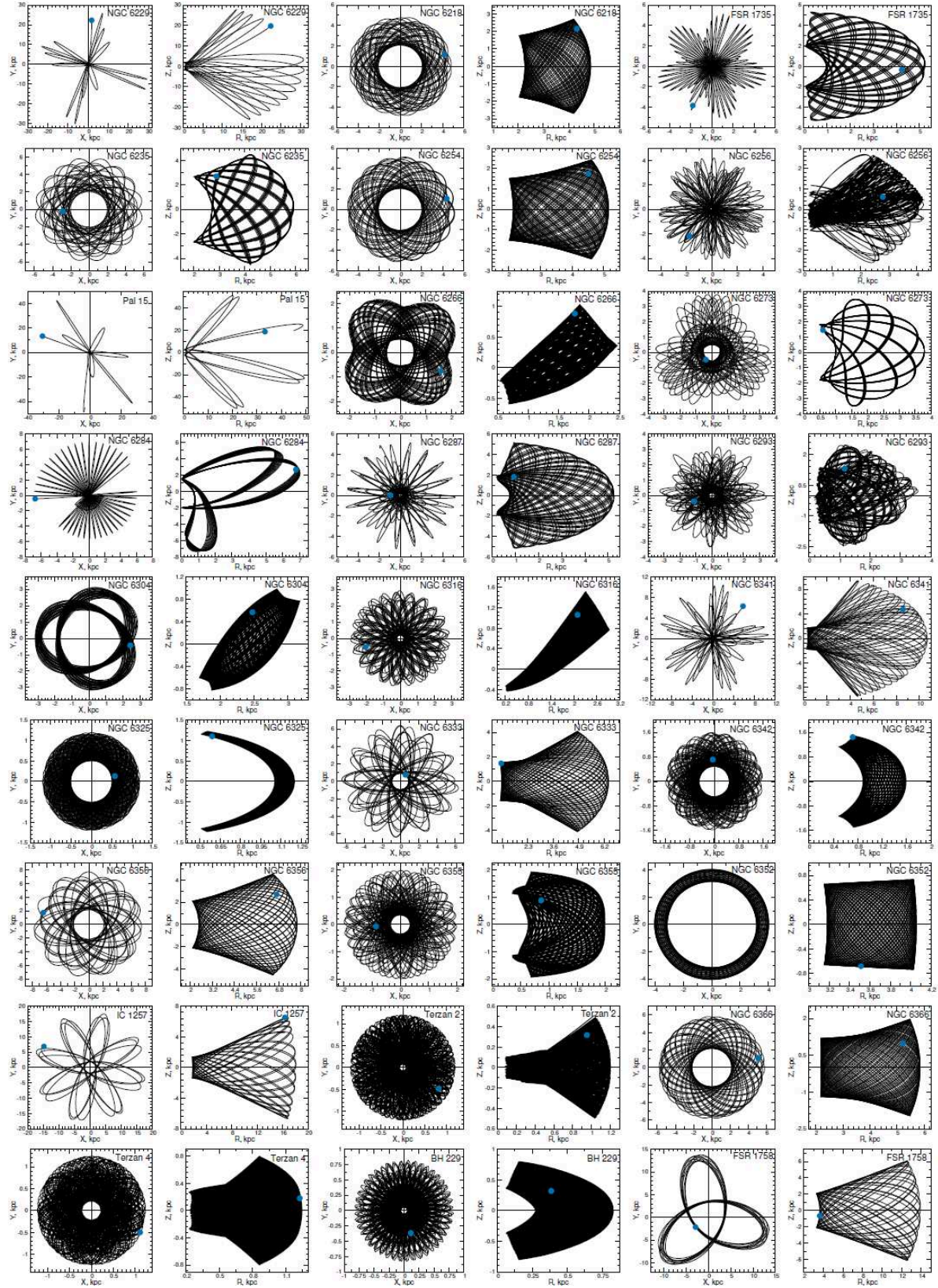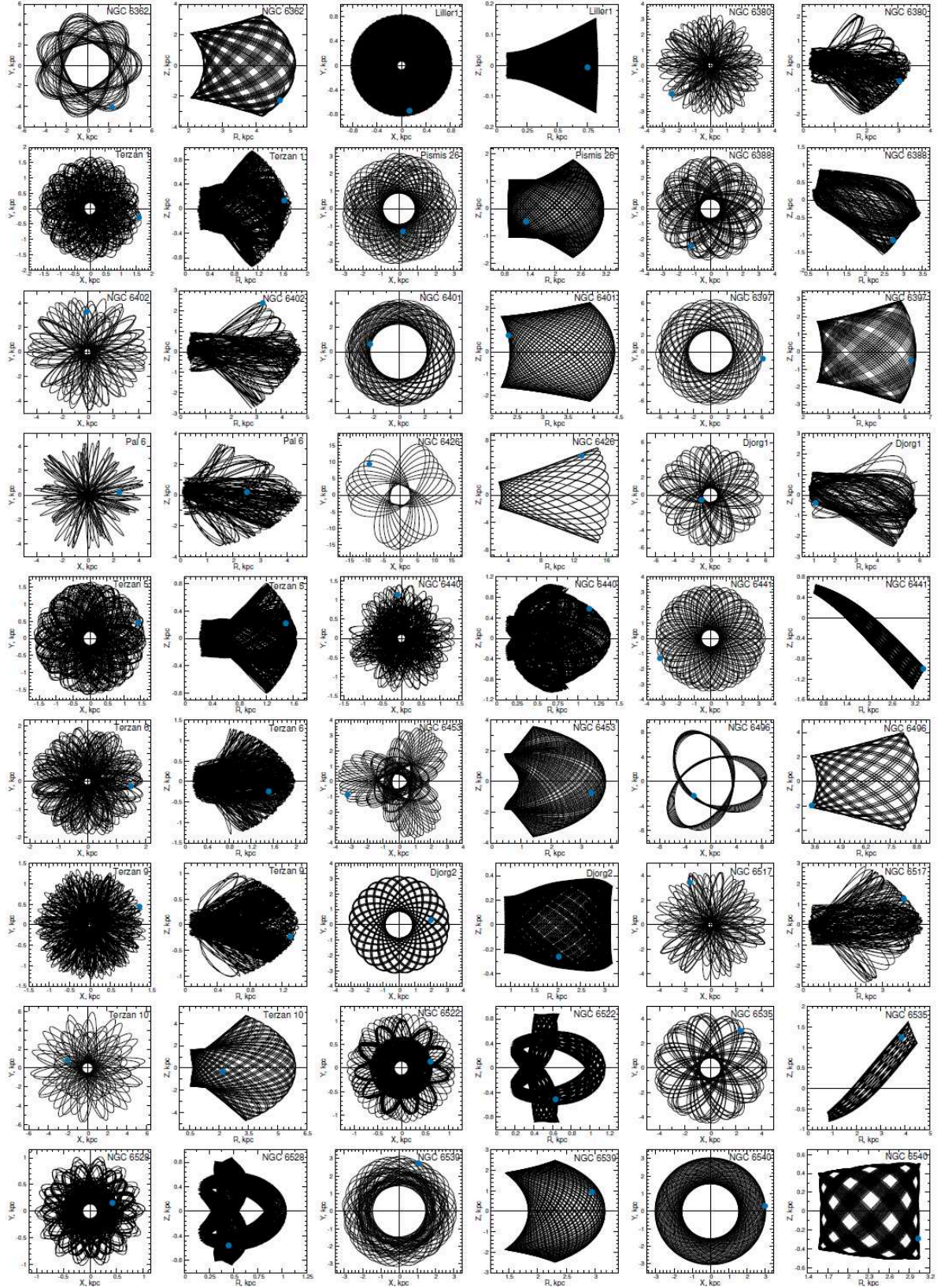
Fig. 2 - continued
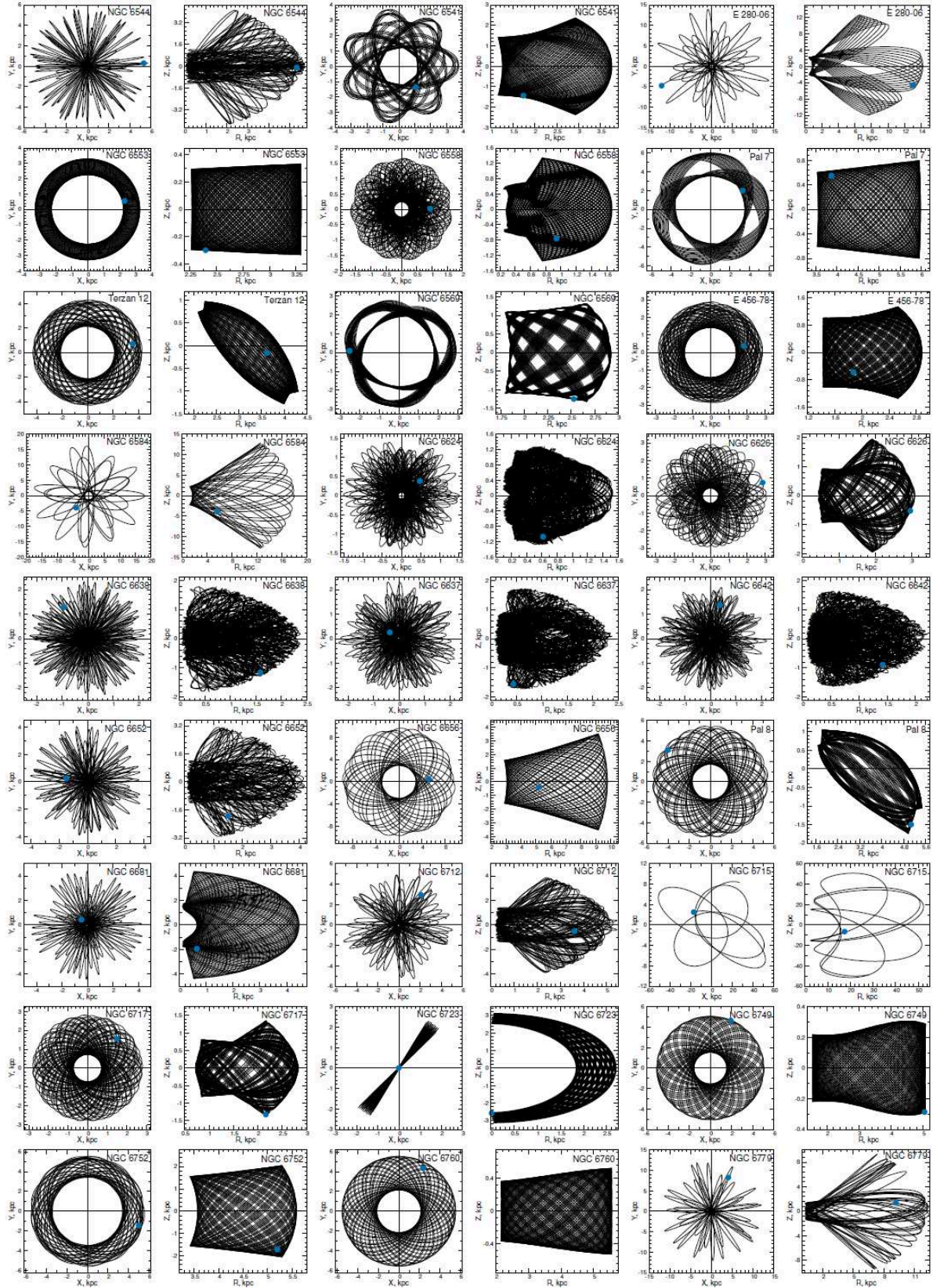
12

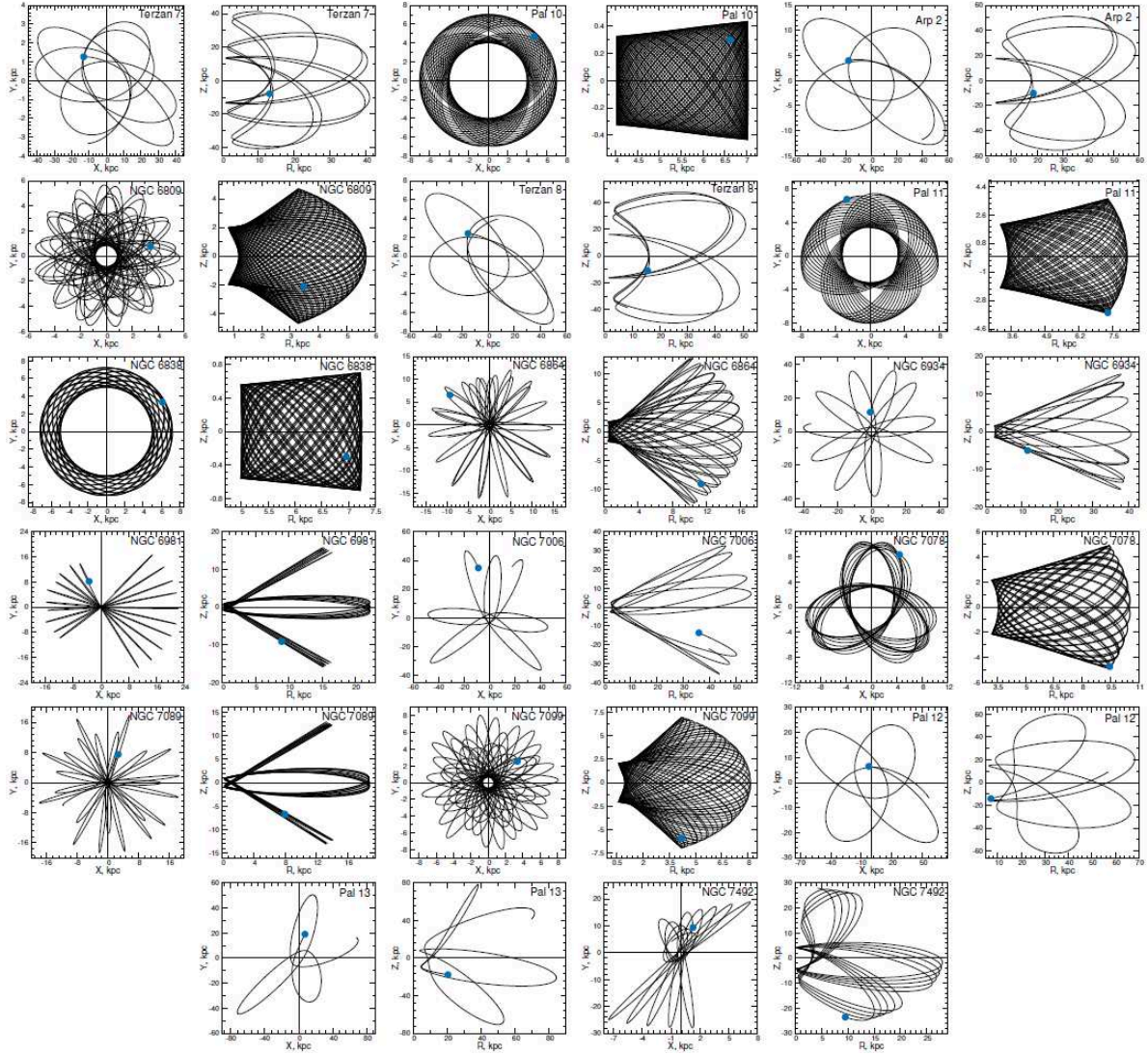Fig. 2 - continued

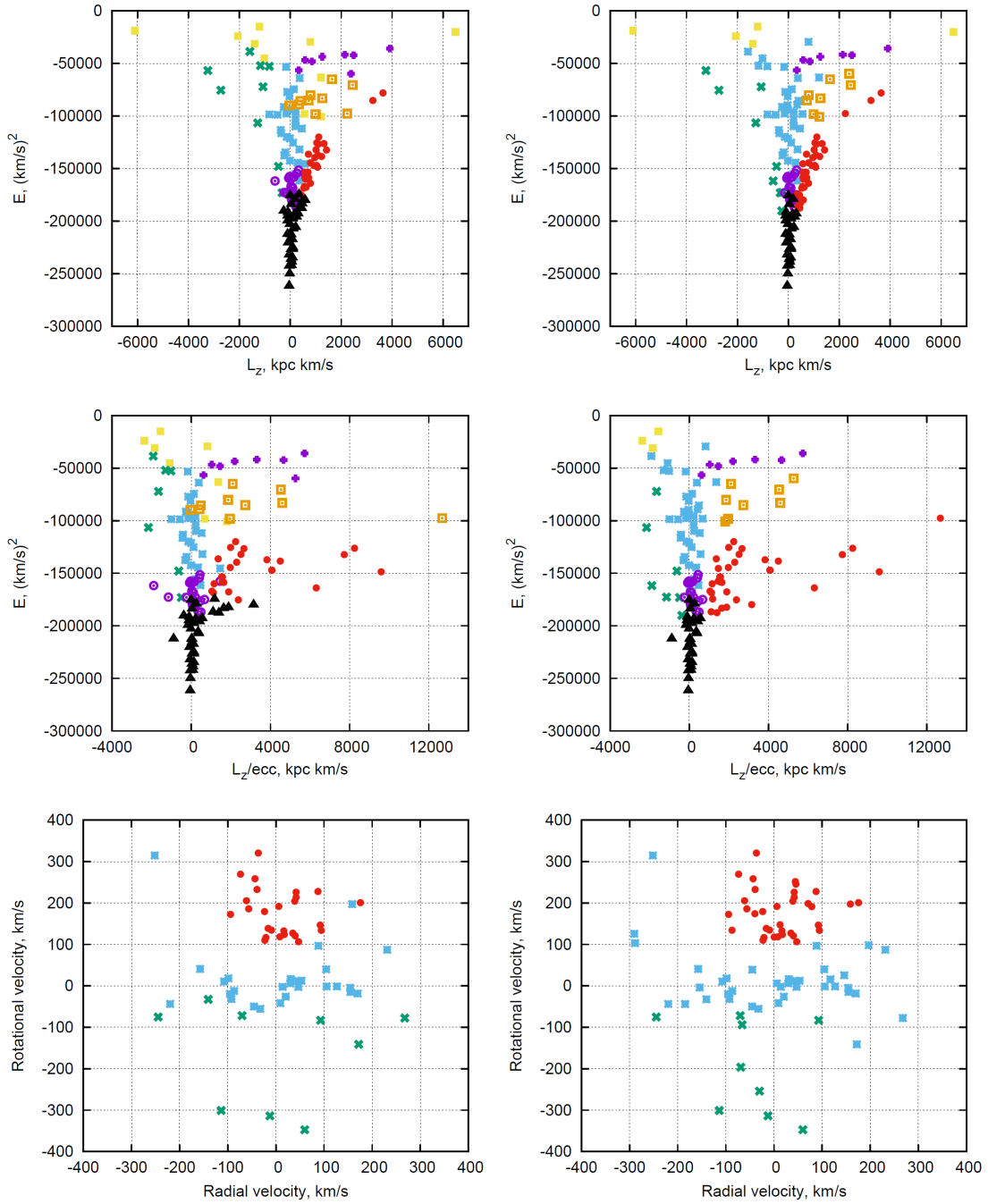Fig. 2 - continued

14

Fig. 2 - continued

15

Fig. 2 - continued

16

Figure 3: The "L_Z – Energy" (top panel), "L_Z/ecc – Energy" (middle panel) and "Radial velocity – Rotational velocity" (bottom panel) diagrams for GCs. Classification by Massari et al. (2019) (left-hand panels); the modified classification (right-hand panels). Colour-coded according to their belonging to different subsystems (red symbols mark the disk, black is for the bulge, blue is for Gaia-Enceladus (Gaia-Sausage), orange for Helmi Streams, green for Sequoia, violet crosses for Sagittarius, yellow for the high-energy group, violet circles for the low-energy group. For visualisation purposes, clusters E 1 with extremely negative L_Z has not been plotted.

7 Acknowledgements

8 References

- Bajkova, A.T. & Bobylev, V.V. 2016, Ast. Lett., 42, 567

- Bajkova, A.T. & Bobylev, V.V. 2017, OAst, 26, 72

- Bajkova, A.T., Carraro, G., Korchagin, V.I., Budanova, N.O. & Bobylev, V.V. 2020, ApJ, 895, 69

- Baumgardt, H., Hilker, M., Sollima, A. & Bellini A. 2019, MNRAS, 482, 5138

- Bhattacharjee, P., Chaudhury, S. & Kundu, S. 2014, ApJ, 785, 63

- Bobylev, V.V. & Bajkova A.T. 2016, Ast. Lett., 42, 1

- Harris, W. 2010, arXiv: 1012.3224

- Gaia Collaboration, Helmi, A., van Leeuwen, F., McMillan, P.J., et al. 2018, A&A, 616, 12

- Irrgang, A., Wilcox, B., Tucker, E. & Schiefelbein, L. 2013, A&A, 549, 137

- Koppelman, H.H. & Helmi, A. 2020, arXiv: 2006.16283

- Massari, D., Koppelman, H. H. & Helmi, A. 2019, A&A, 630, L4

- Miyamoto, M. & Nagai, R. 1975, PASJ, 27, 533

- Myeong, G. C., Vasiliev, E., Iorio, G., Evans, N. W. & Belokurov, V. 2019, MNRAS, 488, 1235

- Navarro, J.F., Frenk, C.S. & White, S.D.M. 1997, ApJ, 490, 493

- Schonrich, R., Binney, J. & Dehnen, W. 2010, MNRAS, 403, 1829

- Vasiliev, E. 2019, MNRAS, 484, 2832

- Villanova, S., Monaco, L., Geisler D., et al. 2019, ApJ, 882, 174